Path-integral simulation of the superfluid transition in two-dimensional ^{4}He

D. M. Ceperley
National Center for Supercomputer Applications, Department of Physics, University of Illinois, Champaign, Illinois 61820

E. L. Pollock
Physics Department, Lawrence Livermore National Laboratory, University of California, Livermore, California 94550
(Received 9 September 1988)

The superfluid transition in a two-dimensional ^{4}He system has been studied using computational-path-integral methods. Thermodynamic and structural properties, the single-particle momentum distribution, the one-particle off-diagonal density matrix (or order-parameter correlation function), the momentum correlations, the superfluid density (based on the winding-number distribution) and the vorticity correlation function were calculated for temperatures above and below the superfluid transition for a film density of 0.0432 Å^{-2} (which corresponds to zero pressure in the ground state). The order-parameter correlation function shows an algebraic decay in good agreement with spin-wave theory. An indirect estimate based on an analysis of finite-size effects using the Kosterlitz-Thouless recursion relations leads to a vortex diameter of 3.7±0.4 Å, a vortex core energy of 2.7±0.2 K and a critical temperature of 0.72±0.02 K.

I. INTRODUCTION

The superfluid transition in bulk three-dimensional ^{4}He is associated with macroscopic occupation of the zero-momentum state (Bose condensation). In ^{4}He films at nonzero temperature there is no Bose condensate; however, a superfluid transition is still observed. In the theory of Kosterlitz and Thouless (KT),[1-4] the transition from superfluid to normal is associated with the unbinding of pairs of vortex excitations with opposite circulation. Unlike the continuous decrease in the superfluid density observed in three dimensions, the theory predicts a universal jump in the superfluid density at the critical temperature. The theory also associates a change in the order-parameter correlation from an algebraic to the usual high-temperature exponential decay with the onset of this vortex unbinding and suggests a bump in the specific heat above the critical temperature due to the gradual dissociation of these vortex pairs. Specifically, the order-parameter correlation below the transition temperature is predicted to decay as $1/r^{\eta}$ with $\eta = mkT/2\pi\hbar^2\rho s$, and the jump in the superfluid density at the transition is

$$\frac{\rho_S(T_c-)}{\rho} = \frac{2m}{\hbar^2}\frac{kT_c}{\pi\rho} . \tag{1}$$

This last prediction is well supported by experiment.[5]

It has recently been shown that path-integral computations can be used to give a microscopic description, based only on an interatomic potential, of the superfluid transition in three dimensions, which agrees with experiment to within the uncertainties of the computations due to Monte Carlo statistical fluctuations and the finite-size effects of the periodic systems used[6] (hereafter referred to as I). In this paper these techniques are used to study the superfluid transition in two dimensions.

In the next section the computational-path-integral method is briefly summarized leaving the details to the references. This method is applied to a periodic two-dimensional system of ^{4}He atoms interacting through the Aziz (HFDHE2) pair potential.[7] A film density of 0.0432 particles/Å^2 was used which corresponds to the zero-pressure density for this system in the ground state.[8] This interparticle spacing is considerably larger than in the zero-pressure three-dimensional system since the kinetic energy is here relatively more important than the potential. In Sec. III the potential and kinetic energy, pressure, and the structural properties are presented. The presence of a superfluid is most fundamentally related to long-ranged momentum correlations. These momentum correlations are discussed in Sec. IV along with the superfluid densities. The finite-size rounding of the transition is analyzed using the KT recursion relations to estimate a vortex diameter of 3.7±0.4 Å and a vortex core energy of 2.7±0.2 K. The Fourier transform of the one-particle off-diagonal density matrix (OPODDM) (which corresponds to the order-parameter correlation) gives the single-particle momentum distribution. These are presented in Sec. V. The OPODDM in two dimensions shows algebraic decay (i.e., inversely proportional to some power of the distance) at low temperature rather than going to a nonzero constant as in three dimensions so the momentum distribution display no macroscopic occupation of the zero-momentum state although it is singular at zero momentum (considerably less so than the 2D ideal Bose gas, however). The computed algebraic decay of the OPODDM at low temperature is in good agreement with the spin-wave prediction using the computed superfluid densities. In Sec. VI an attempt is made to see the vortex unbinding, proposed as the underlying mechanism in the superfluid transition, directly by computing the vorticity correlation function. No direct indication of such a transition is seen.

II. COMPUTATIONAL ASPECTS

Path integrals, introduced by Feynman[9] in his theory of the three-dimensional superfluid transition, are increasingly being used in the computer simulation of realistic quantum many-body systems. The basic discretized path-integral formula is derived by inserting complete sets of states into the following identity for the many-body density operator:

$$e^{-\beta H}=(e^{-\tau H})^{L}\ , \tag{2}$$

written here for an inverse temperature or "imaginary time" $\beta\equiv 1/k_B T$ with $\tau=\beta/L$. In real space this gives an expression for the density matrix

$$\rho(R,R';\beta)=\langle R\mid e^{-\beta H}\mid R'\rangle$$
$$=\int\cdots\int\rho(R,R_1;\tau)\rho(R_1,R_2;\tau)\cdots\rho(R_{L-1},R';\tau)dR_1dR_2\cdots dR_{L-1}\ , \tag{3}$$

as a sum over all discretized paths of terms involving the density matrix at a higher temperature. In the preceding equation R denotes a dN-dimensional vector for an N particle system in d dimensions. Bose statistics are introduced by symmetrization

$$\rho_{\text{Bose}}(R,R';\beta)=\frac{1}{N!}\sum_{\mathcal{P}}\rho(R,\mathcal{P}R';\beta)\ , \tag{4}$$

over permutations, $\mathcal{P}$, in an N particle system.

The density matrices in Eq. (3) correspond to a higher temperature (shorter "imaginary time") so that for sufficiently small τ an accurate approximation for these high-temperature density matrices may be used. Here, and in previous work on superfluid ^{4}He, a pair product approximation was used for this.[10] The error in this approximation may be shown to decrease as τ^3.[11] A value of τ corresponding to 1/40 K has been found to give results accurate to within the statistical errors of the Monte Carlo methods employed in these computations. The pair-density matrix entering this approximation was computed from the 2D Bloch equation for the Aziz potential. Details of the Monte Carlo computations may be found in Refs. 6 and 11. As discussed in I, the superfluid densities were calculated based on the mean-squared number of times the paths in the path integral wound around the periodic cell. Generating path configurations with a nonzero winding number requires a global move which restricts the system size for which superfluid densities can be computed. In the superfluid density computations a periodic system of 25 particles was used. There is no such restriction in computing the single-particle momentum distribution, so 62 atoms in the periodic cell were used for these.

A typical path configuration is shown for a $T=2.5$ K system in Fig. 1. Here four cells of the infinite periodic system are shown. In this snapshot the arrows are directed between every second point on the individual particle paths. (Plotting every point on the particle paths gives a more confusing plot.) The solid dots give the particle positions at what is arbitrarily taken as the imaginary time zero. The size of the particle paths is given roughly by the thermal deBroglie wavelength. At $T=2.5$ K this size is much less than the average interparticle spacing and consequently there are no permutations. Only the identity permutation contributes in Eq. (4).

In Fig. 2 for a temperature $T=0.8$ K near the superfluid transition, the particle paths overlap and numerous permutations are seen since the paths of many particles may now interconnect. This configuration has a winding number of 1 in both the x and the y directions. The winding path is highlighted in the figure. In interpreting these paths according to Eq. (3), it is seen that particles only interact with other particles at the same "imaginary time" or at adjacent "imaginary times." For example, R_2 only appears with R_1 and R_3 in the integrand of Eq. (3) and not with the other R's. So unlike the picture of a system of classical polymers, the paths here can cross themselves in 2D. A three-dimensional plot with imaginary time as the third dimension would make this clearer. At high temperature where the thermal deBroglie wavelength is shorter than the range of the interaction, such crossings are rare, but at low temperature they become very frequent.

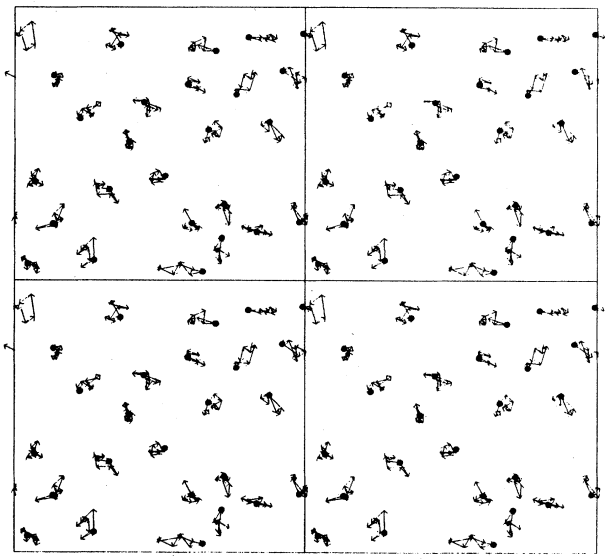

FIG. 1. Typical path configuration at $T=2.5$ K. Arrows connect every second point on the individual particle path. The solid dots give the various particle positions at the same "imaginary time" instant. Four cells of the periodic system are shown.

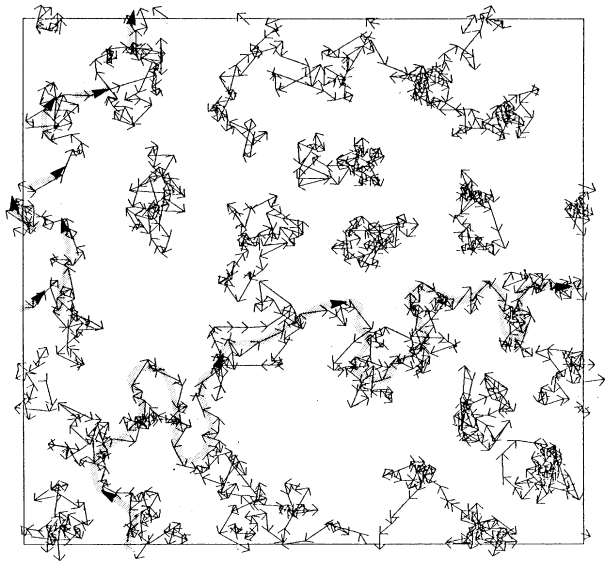

FIG. 2. Typical path configuration at $T=0.8$ K. Only one periodic cell is shown here. The dark arrowheads and light-gray line indicate a path winding across the unit cell in both the x and y directions.

III. THERMODYNAMIC AND STRUCTURAL PROPERTIES

The various averages giving the thermodynamic and structural properties may be straightforwardly computed from the many-body density matrix as discussed in I and in the references. The kinetic, potential, and total energies and pressures are compiled in Table I.

Figure 3 shows the total energy as a function of temperature. At sufficiently low temperature, phonons are the only excitations and the energy approaches

$$E=E_0+c_3T^3+\cdots , \tag{5}$$

where

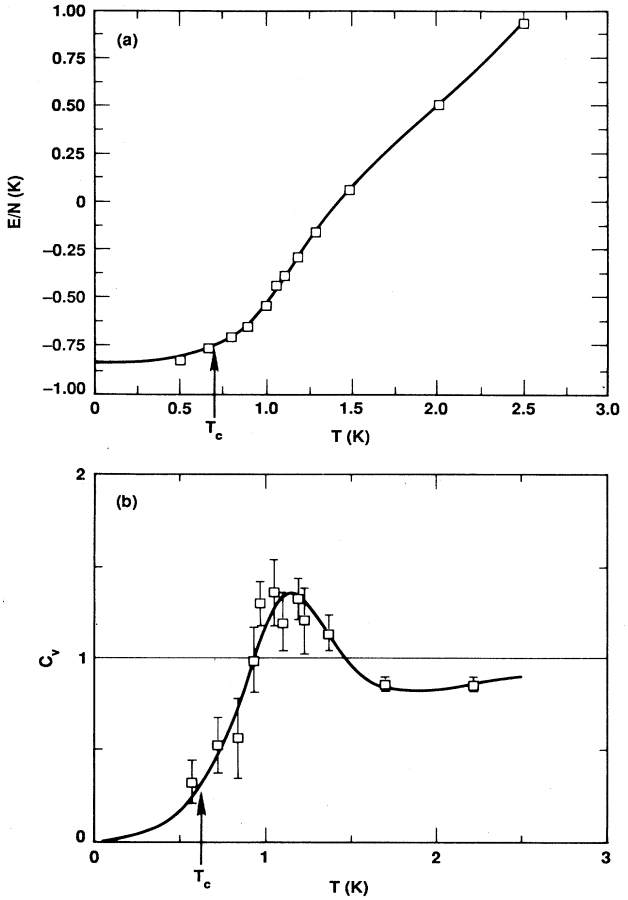

FIG. 3. (a) Total energy per particle in K vs temperature. The squares are data from Table I. The line is a (5,4) Padé fit to the data with the high- and low-temperature forms as constraints. The arrow gives the approximate location (see Sec. IV) of the Kosterlitz-Thouless transition. (b) The specific heat vs temperature. The squares with error bars are obtained by differencing the energies of Table I while the line is the derivative of the Padé fit to the energies.

TABLE I. Summary of simulation results for 2D ^{4}He film with surface density $\rho=0.0432$ Å^{-2} and $N=25$ particles in the periodic cell. The kinetic $\langle KE\rangle$, potential $\langle U\rangle$, and total energies $\langle E\rangle$ are in K. The surface pressure $\langle P\rangle$ is in K/Å^2. The statistical uncertainty in the least significant figure is given in parentheses. The $T=0.0$ K values are quoted from Ref. 8.

T (K)	$\langle P\rangle$	$\langle KE\rangle$	$\langle U\rangle$	$\langle E\rangle$	ρ_s/ρ	$g^{\max}(r)$
0.00	−0.001	3.9(1)	−4.7(1)	−0.85(3)	1.0	1.23
0.50	0.0038(2)	3.977(6)	−4.795(4)	−0.818(5)	0.94(8)	1.25
0.667	0.0049(2)	4.053(9)	−4.824(5)	−0.771(6)	1.00(8)	1.26
0.80	0.0062(2)	4.168(9)	−4.869(5)	−0.701(7)	0.82(7)	1.275
0.889	0.0071(2)	4.235(9)	−4.886(5)	−0.651(9)	0.69(10)	1.281
1.00	0.0086(1)	4.375(9)	−4.916(4)	−0.541(7)	0.59(5)	1.288
1.053	0.0096(2)	4.497(9)	−4.936(6)	−0.438(9)	0.44(6)	1.295
1.111	0.0104(1)	4.571(9)	−4.961(4)	−0.390(7)	0.35(4)	1.301
1.177	0.0116(2)	4.688(9)	−4.978(5)	−0.290(7)	0.27(5)	1.306
1.290	0.0132(1)	4.860(9)	−5.013(5)	−0.153(6)	0.15(3)	1.316
1.48	0.0164(2)	5.118(9)	−5.055(5)	0.064(6)	0.015(10)	1.329
2.0	0.0237(4)	5.67(2)	−5.17(1)	0.51(1)	0.0	1.356
2.5	0.0317(4)	6.18(2)	−5.25(1)	0.94(1)	0.0	1.379

$$c_3=\frac{\zeta(3)\kappa m}{\pi\rho\hbar^2}=0.20\ \mathrm{K}^{-2}\ . \tag{6}$$

The value of the ground-state compressibility κ used in evaluating Eq. (6) is taken from Ref. 8. At high temperature the energy approaches T+const. A (5,4) Pade in T was χ^2 fitted to the computed energies using the high- and low-temperature forms as constraints. The result is the solid line in Fig. 3(a). The specific heat obtained by differentiating this curve is displayed in Fig. 3(b). It has a maximum at $T=1.15$ K. In the KT theory the specific heat has only an unobservable essential singularity at T_c and a maximum above this due to the entropy increase as the vortices unbind. The energies of Fig. 1 are thus consistent with the zero-temperature results of Ref. 8 and the known high- and low-temperature forms.

The radial distribution functions for the 2D system at $T=0.5$, 1.1, and 2.0 K (all at $\rho=0.0432$ Å^{-2}) are compared in Fig. 4 with a previously computed 3D result[10] at $\rho=0.02182$ Å^{-3} which corresponds to approximately zero pressure in 3D. In zero pressure the atoms are about 20% farther apart in 2D than they are in 3D. This is because the kinetic energy at the same interparticle spacing is larger relative to the potential energy in 2D than in 3D, by geometry, hence at zero pressure the 2D system is less dense with correspondingly slightly less structure in $g(r)$.

Figure 5 shows a purely theoretical construct, the isocyclic radial distribution function. This is the usual radial distribution function but now only counting particles on the same permutation cycle [see Eq. (4)]. This demonstrates rather strikingly the increase in number and length of the permutation cycles which are responsible for the superfluid transition.

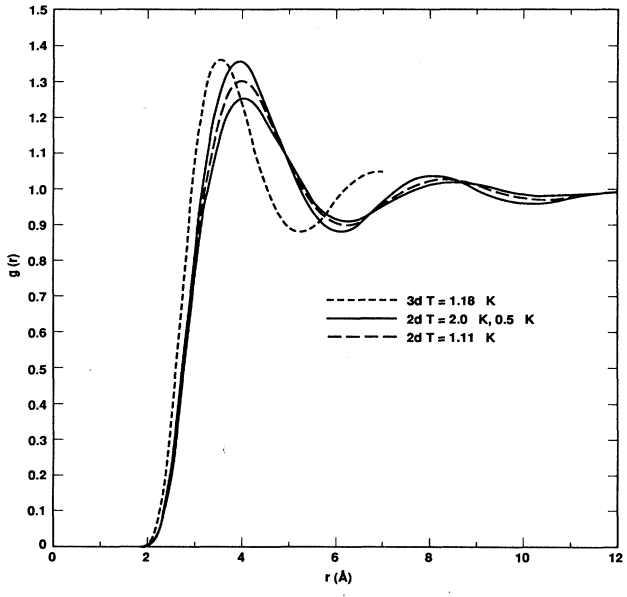

FIG. 4. Radial distribution functions in 2D for $T=0.5$ K (lower solid line), $T=1.11$ K (long-dashed line), $T=2.0$ K (upper solid line) and in 3D for $T=1.18$ K and zero pressure (short-dashed line).

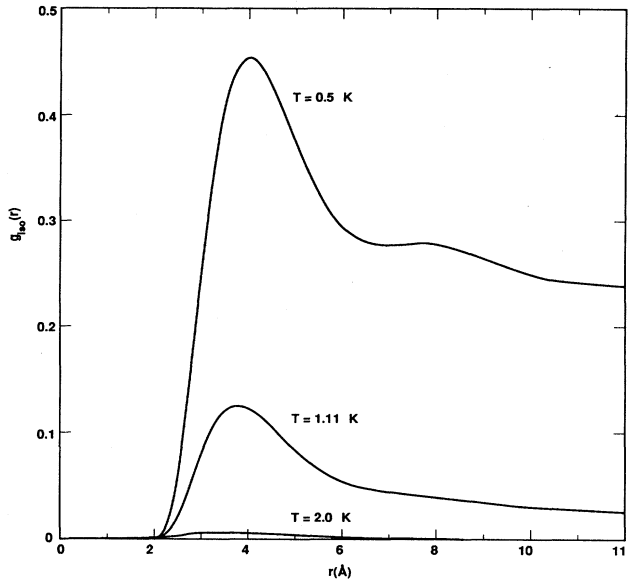

FIG. 5. Isocyclic radial distribution function at $T=0.5$, 1.11, and 2.0 K. In the isocyclic $g(r)$ only particles at a distance r from the central particle and on the same permutation cycle are counted.

Figure 6 shows in detail the probabilities for the various exchange processes (or permutation cycle lengths). $P_n(T)$ is the probability an atom is on a cycle of length n, normalized as $1=\sum_{n=1}^{N}P_n(T)$. At zero temperature an atom is equally likely to be on a permutation cycle of any length [$P_n(0)=1/N$ for an N particle system].

IV. MOMENTUM CORRELATIONS AND SUPERFLUID DENSITY

The existence of superfluidity is signaled by the onset of long-range order in the momentum-density correlation function. A discussion of this connection and a derivation of the equivalent winding number estimator for the superfluid fraction is given in I and references therein.

The momentum-density correlation function may be written

$$\overleftrightarrow{G}(\mathbf{r})=\langle\mathbf{p}(\mathbf{r})\cdot\mathbf{p}(0)\rangle$$
$$=[m\rho\langle K\rangle\delta(\mathbf{r})+G_N(r)]\overleftrightarrow{I}+G_S(r)\frac{2\hat{\mathbf{r}}\hat{\mathbf{r}}-\overleftrightarrow{I}}{r^2}\ , \tag{7}$$

where the self-term is given by the kinetic energy $\langle K\rangle$ and the momentum density

$$\mathbf{p}(\mathbf{r})=\frac{\hbar}{2m}\sum_j\nabla_j\delta(\mathbf{r}-\mathbf{r}_j)+\delta(\mathbf{r}-\mathbf{r}_j)\nabla_j\ . \tag{8}$$

The functions $G_N(r)$ and $G_S(r)$ defined by this equation are related to the superfluid density by

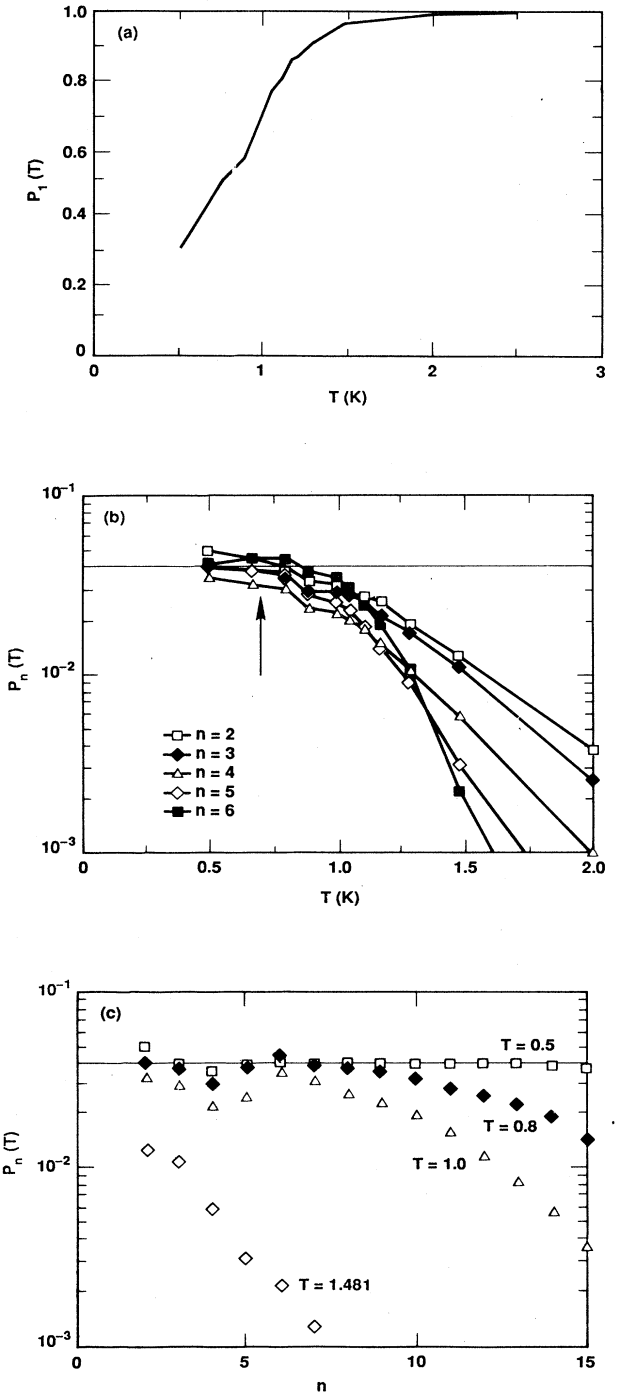

FIG. 6. (a) $P_1(T)$, the probability an atom is not involved in an exchange. At $T \approx 0.7$ K $\approx T_c$, only about $\frac{1}{2}$ of the atoms are involved in exchanges. At high temperature $T > 1.5$ K, the exchanges are thermally activated, while at low temperature $P_1(T)$ is linear. (b) $P_N(T)$ for $n = 2$–6. At high temperature each segment in the exchange path costs energy (E_s) and $P_n(T) \propto e^{-n\beta E_s}$. (c) Plot of cycle length distributions at 4 temperatures for $N = 25$. At the lowest temperature 2 particle exchanges are slightly favored. At zero temperature all cycle lengths would be equally probable [$P_l(T) \to 1/N = 0.04$].

$$\rho_N = \frac{\beta}{2m} \int \langle \mathbf{p}(\mathbf{r}) \cdot \mathbf{p}(0) \rangle dr^2 = \rho \left[\beta \langle K \rangle + \int 2\pi\rho r \frac{G_N(r)}{mkT\rho^2} dr \right] , \tag{9}$$

and

$$G_S(r) \to -\rho_S \frac{mkT}{2\pi} . \tag{10}$$

It is interesting to note that, in the limit of small imaginary time steps ($\tau \to 0$), the momentum-density autocorrelation function is given by the correlation between the directed path segments. Using Eqs. 38 and 39 of I,

$$\vec{G}(\mathbf{r}) = \frac{-2m^2}{\hbar^2} \rho \left\langle \frac{1}{N} \sum_{i,j<j} \frac{d\mathbf{r}_i}{d\tau} \frac{d\mathbf{r}_j}{d\tau} \delta(\mathbf{r} - \mathbf{r}_{ij}) \right\rangle , \tag{11}$$

where $d\mathbf{r}/d\tau$ is the path segment length divided by the imaginary time step. Thus the path segments in, for example, Figs. 1 and 2 can, when divided by the imaginary time step, be viewed as a "velocity" field in calculating the momentum correlations and superfluid densities. Within one polymer the direction of the arrows can be reversed to generate an equally likely configuration assuming this polymer is not too close to another polymer. But this reverses the relative velocity with particles on other polymer loops, thus the main contribution to $\vec{G}$ comes from pairs of atoms on the same polymer loop. Thus a superfluid response is only possible when there are long polymers involving many particles present.

Figure 7, showing $2\pi G_N(r)/mkT\rho$ and $2\pi G_S(r)/mkT\rho$ for temperatures below and above the superfluid transition temperature, demonstrates the change in the large r behavior of $G_S(r)$. The $G_N(r)$ component is qualitatively unchanged through the transition. These curves are similar to those for the 3D system.[6]

Another display of the momentum-density correlation function is given by the vector-field plot in Fig. 8. The short-range correlations are negative, which from Eq. (9) is needed to reduce the normal fraction below 1 since $\beta\langle K \rangle$ is always greater than 1 (see Table I). The weak dipolar field at large r is, from Eq. (10), only present in the superfluid case.

It is difficult to accurately estimate ρ_S from the larger r behavior of the $G_S(r)$ curves above. The superfluid fractions given in Table I were obtained from the mean-squared winding number, $\mathbf{W}$, defined by

$$\sum_{i=1}^{N} (\mathbf{r}_{\rho_i} - \mathbf{r}_i) = \mathbf{W}L , \tag{12}$$

where L is the periodic cell length, through the relation

$$\frac{\rho_S}{\rho} = \frac{m}{\hbar^2} \frac{\langle W^2 \rangle}{2\rho\beta} , \tag{13}$$

as derived in I. These are displayed in Fig. 9 along with the solid line indicating the universal jump in the superfluid fraction for a large system. This universal jump formula implies that the mean-squared winding number, $\langle W^2 \rangle$ jumps from 0 to $4/\pi$ at the transition in an infinite system. The finite-size effects for the periodic

system cause considerable rounding of this transition.

It has been suggested that finite-size effects in ^{4}He films may be accounted for in the Kosterlitz-Thouless recursion relations by restricting the maximum separation of the vortex pairs, assumed responsible for the superfluid decrease (or dielectric shielding in the analogous Coulomb gas model) to the system size.[12] Applying this idea to the present simulations gives the dashed line in Fig. 9.

Specifically the KT recursion relations

$$\frac{dK^{-1}(l)}{dl}=4\pi^3 y^2(l)\ ,$$
$$\frac{dy(l)}{dl}=[2-\pi K(l)]y(l)\ , \tag{14}$$

are integrated to $l\equiv\ln(r/d)=\ln(L/2d)$ rather than to ∞. Here,

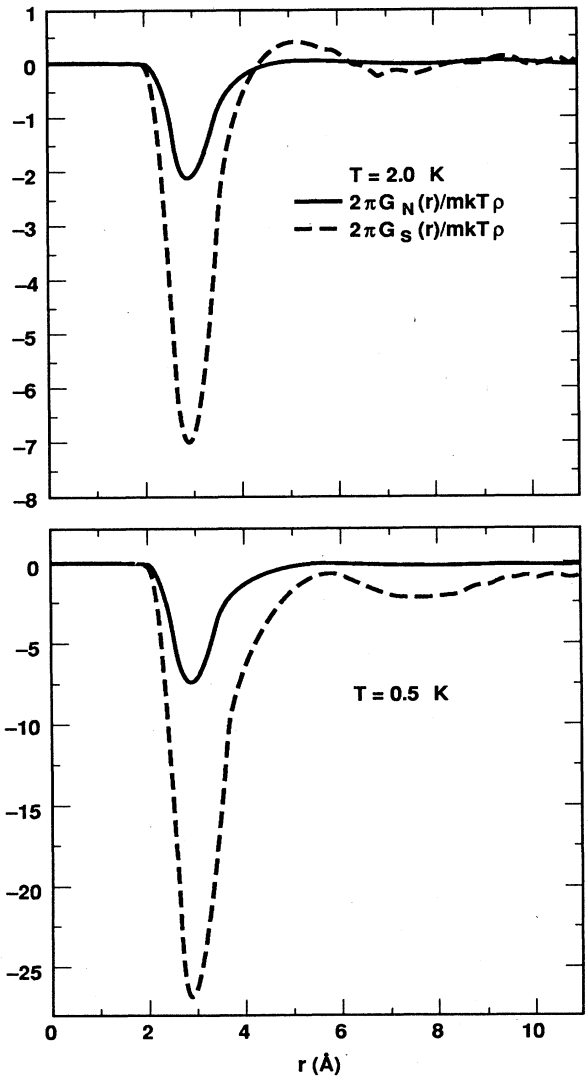

FIG. 7. $2\pi G_N(r)/mkT\rho$ in Å^{-2} (solid line) and $2\pi G_S(R)/mkT\rho$ (dashed line) at $T=2.0$ K and $T=0.5$ K.

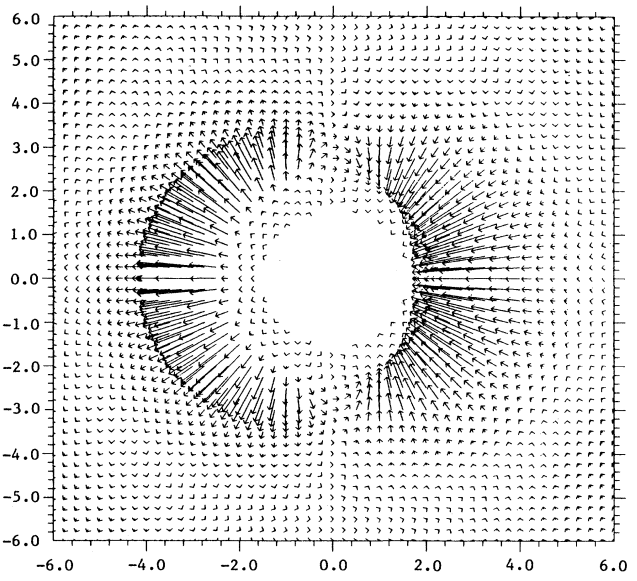

FIG. 8. Plot of $r^2\overleftrightarrow{G}/mkT\rho^2$ at $T=0.5$ K. The vector field components at each $\mathbf{r}$ are $r^2[G_{xx}(\mathbf{r}),\ G_{xy}(\mathbf{r})]/mkT\rho^2$. Lengths are in Å.

$$K(l)=\hbar^2\rho_S(l)/mkT\ ,$$

and the initial values are

$$K(l=0)=\hbar^2\rho/mkT\ ,$$

(with $\rho=0.0432$ particles/Å^2 for these simulations), and

$$y(l=0)=\exp(-\beta E_c)\ .$$

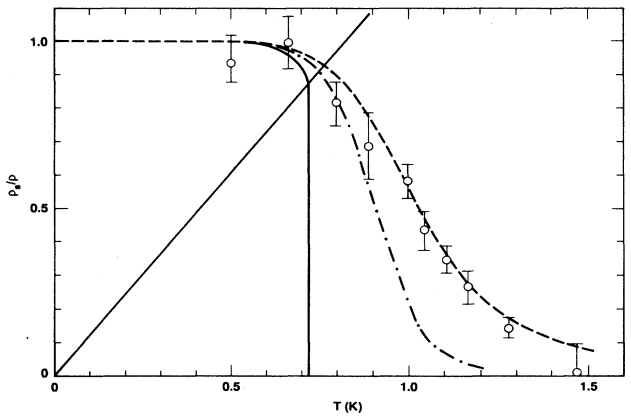

FIG. 9. Graph of computed superfluid fractions (open circles) for a periodic system of $N=25$ particles. The solid line from the origin is the universal jump condition, Eq. (1). The long dashed line is a least-squares fit to the data using the KT recursion relations. This gave a best fit vortex diameter of 3.7±4 Å and core energy of 2.7±0.2 K. The dot-dashed line is the predicted superfluid fraction for a periodic system of $N=100$ particles using the recursion relations with the best fit parameters determined from the $N=25$ simulation results. The solid curve is the infinite system result for these parameters giving a transition temperature $T_c=0.72$ K.

The "vortex core diameter" d and "vortex core energy" E_c were obtained by a least-squares fit of the solution of Eq. (14) to the data of Table I to give $d=3.7\pm0.4$ Å and $E_c=2.7\pm0.2$ K. Since these parameters should not change with system size, it is possible to estimate the results of simulations on larger systems. For example, the case of 100 particles in the periodic cell is indicated by the dot-dashed line in Fig. 8.[13] Using these parameters, the critical temperature is estimated as $T_c=0.72\pm0.02$.

Clearly, this analysis of finite-size effects, as well as the estimates for d and E_c, are approximate. The procedure described earlier does not distinguish periodic boundary conditions from a finite system in vacuum (aside from using $L/2$ rather than a length closer to L for the vortex separation cut off) and the KT relations are derived for the case of low vortex density. There is thus an ambiguity in the definition of d, but the goodness of the fit is remarkable. Our estimated T_c agrees with the experimental value of $T_c=0.75$ K at $\rho=0.0460$ Å^2 (Ref. 14).

Since the full many-body density matrix is available from the simulation, it should be possible to study, directly, the equilibrium vortices, but a method for this has not been determined. A first attempt along these lines is made in the last section.

V. ORDER-PARAMETER CORRELATIONS AND THE SINGLE-PARTICLE MOMENTUM DISTRIBUTION

The single-particle momentum distribution, which results from writing the many-body density matrix in momentum space and integrating out all the particle momenta but one,

$$\tilde{n}(k)=\int n(r)e^{-i\mathbf{k}\cdot\mathbf{r}}\frac{d\mathbf{r}^2}{(2\pi)^2}\ , \tag{15}$$

is the Fourier transform of the one-particle off-diagonal density matrix

$$n(r)=\frac{1}{Z}\int \rho(\mathbf{r}_1,\mathbf{r}_2,\ldots,\mathbf{r}_N,\mathbf{r}_1+r,\mathbf{r}_2,\ldots,\mathbf{r}_N;\beta)d\mathbf{r}_1 d\mathbf{r}_2\cdots d\mathbf{r}_N\ , \tag{16}$$

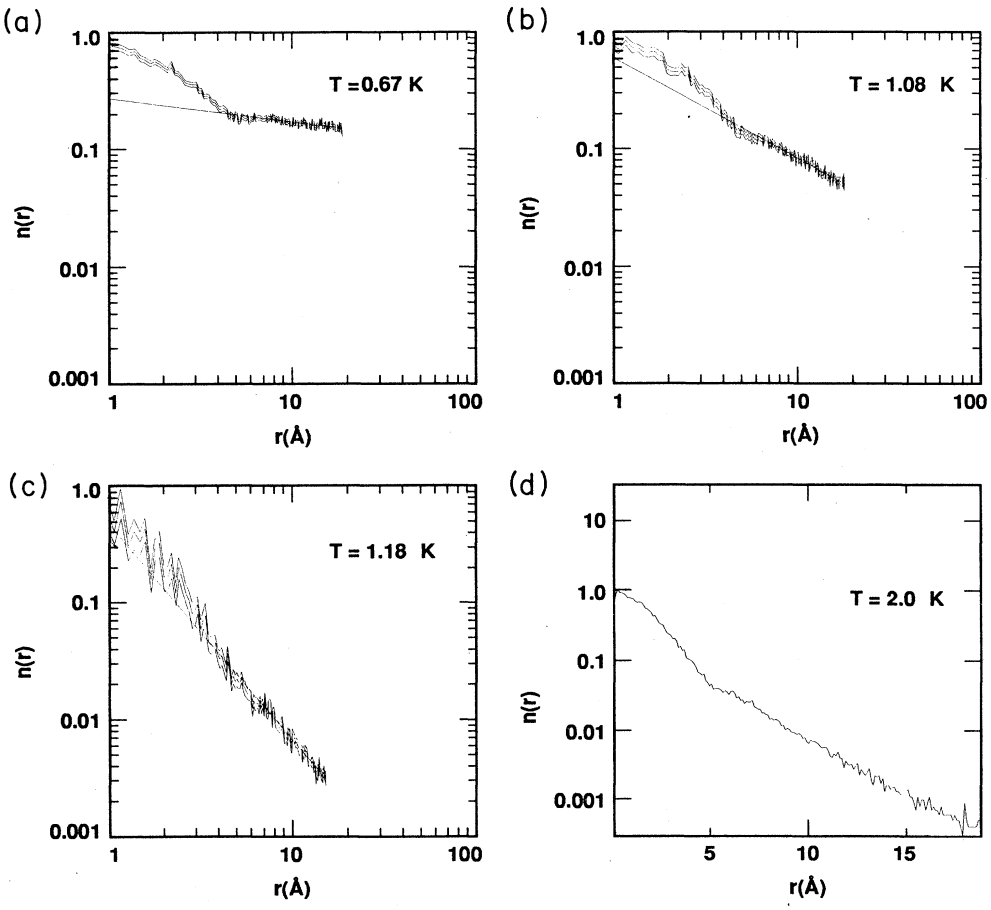

FIG. 10. One-particle off-diagonal density matrices at the indicated temperatures. The upper and lower solid curves in a, b, and c indicate the estimated statistical uncertainty. The solid line in a, b, and c is a fit to the data for $r>6.0$ to the form $n(r)=ar^{-\eta}$. A semilog plot is used for the highest temperature case, $T=2.0$ K, Fig. 10(d).

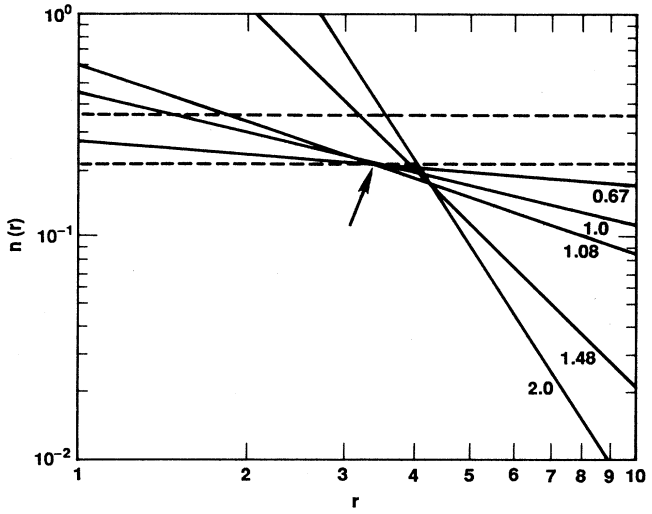

FIG. 11. Asymptotes for the one-particle off-diagonal density matrix at the indicated temperatures (solid lines). The dashed lines give the estimated upper and lower bounds for the zero temperature condensate fraction computed in Ref. 11. The asymptotes for the three lowest temperatures intersect (indicated by arrow) at $r \approx d = 3.7$ Å at a value of ≈ 0.22.

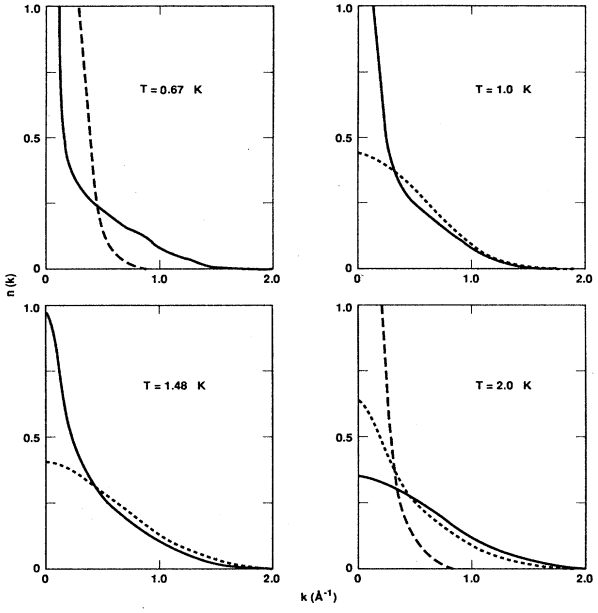

FIG. 12. Single-particle momentum distributions at the indicated temperatures (solid lines). The long-dashed lines are for the ideal Bose gas. The short-dashed lines are for the Gaussian approximation of Eq. (17).

where $\mathcal{Z}$ is the partition function and insures that $n(0)=1.0$. In the path-integral picture $rn(r)$ is proportional to the end to end distribution for a set of paths where one path is not closed but has free ends. A fuller discussion is given in Ref. 15. As first detailed by Penrose and Onsager,[16] $n(r)$ also describes the correlation function for the macroscopic wave function for the system.

Figure 10 displays the computed $n(r)$ with error bars (the upper and lower solid curves) at several indicated temperatures. The solid line in 10(a), 10(b), and 10(c) indicates a least-squares fit for the algebraic decay $[n(r)=Ar^{-\eta}]$ to the large-r part of the curves. Recall that in 3D, $n(r)$ goes to a constant value giving the condensate fraction (percentage of particles in the zero-momentum state).[10] For the $T=2.0$ K case, Fig. 10(d), the large-r ($r>6$) data is slightly better fitted by $n(r)=Ae^{-r/\xi}$ with $\xi=2.8$ Å.

Values for η obtained this way are given in Table II herein and compared with the spin-wave prediction $\eta=mkT/2\pi\hbar^2\rho_S$ using the computed ρ_S values from Table I.

According to the universal jump formula, Eq. (1), $\eta=0.25$ at the transition in a large system. The agreement between η based on $n(r)$ and the spin-wave prediction is remarkable, extending out to temperatures where η is as large as 1.

Figure 11 shows the asymptotic form of $n(r)$ at several indicated temperatures. It is seen that the low-temperature $n(r)$'s come together at $r \approx d = 3.7$ Å and $n(d) \approx 0.22$. This value is consistent with the zero-temperature condensate fraction calculated with Green's Function Monte Carlo ($0.36 > n_0 > 0.22$).[8]

Figure 12 displays the single-particle momentum distributions obtained by transforming the $n(r)$ of Fig. 10. There is no momentum condensate in these systems but the distribution is singular at low wave vector although considerably less so than the ideal Bose gas shown for comparison by the dashed lines at the highest and lowest temperature. The dot dashed line in Figs. 12(b), 12(c), and 12(d) are for the Gaussian approximation

$$n(k)=\frac{\hbar^2}{2\pi m\langle K\rangle}\exp(-\hbar^2k^2/2m\langle K\rangle)\ . \tag{17}$$

For 3D ^{4}He at saturated vapor pressure (SVP), this approximation gives a much closer description to the non-condensed part of the momentum distribution.

TABLE II. Comparison of the algebraic decay exponent of the computed order parameter correlation with the spin-wave-theory prediction.

T (K)	0.666	1.0	1.08	1.18	1.48	2.0
η	0.19(3)	0.59	0.85(4)	1.94	2.5(2)	3.9
$mkT/2\pi\hbar^2\rho_S$	0.21(3)	0.52(4)	0.82(5)	1.3(3)		
A	0.27	0.45	0.60	0.46	6.2	49.0

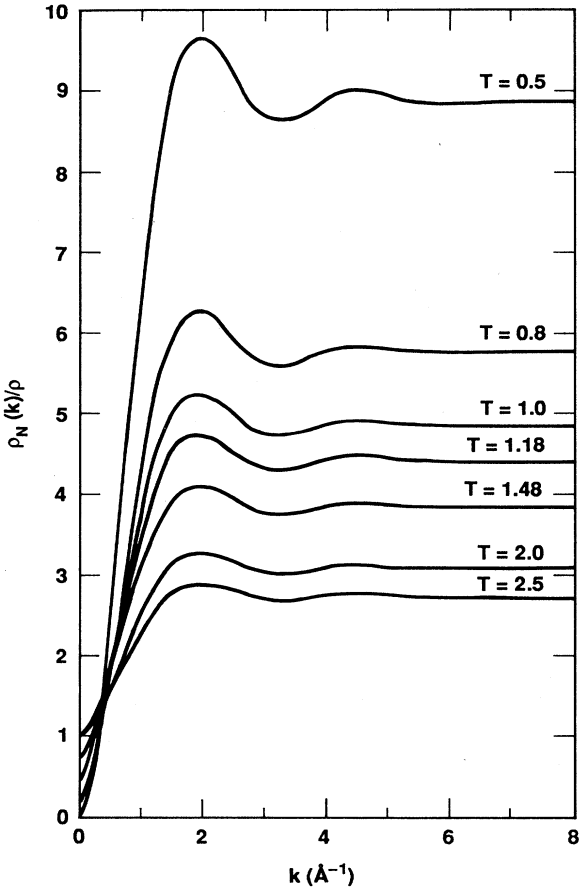

FIG. 13. $\rho_N(k)/\rho$ for the indicated temperature (in K).

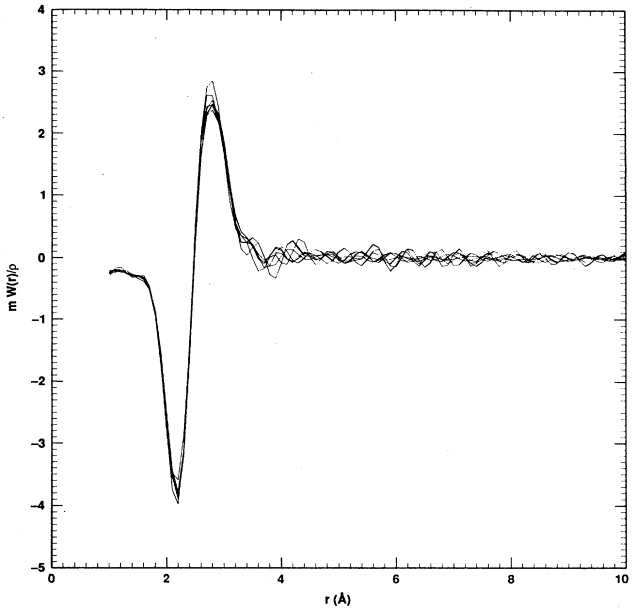

FIG. 14. Vorticity density correlation function $mW(r)/\rho$ (in $K\text{Å}^{-4}$) for the temperatures of Fig. 13. The two highest peaks at $r\approx 3.0$ correspond to $T=2.0$ K and $T=2.5$ K.

VI. VORTICITY CORRELATION FUNCTION

In order to see directly the proposed vortex-unbinding mechanism, the vorticity density correlation function was computed. Based on the vortex-unbinding picture one might anticipate a single well-defined negative peak at temperatures below the transition corresponding to bound vortices of opposite circulation separated by some distance greater than the core diameter. Above the transition temperature this peak should broaden as the vortices unbind.

Using the usual definition of vorticity density

$$\mathbf{\Gamma}(\mathbf{r})\equiv\nabla\times\frac{\mathbf{p}(\mathbf{r})}{m}\ , \tag{18}$$

the vorticity density correlation function

$$W(\mathbf{r}-\mathbf{r}')=W(|\mathbf{r}-\mathbf{r}'|)\equiv\langle\mathbf{\Gamma}(\mathbf{r})\cdot\mathbf{\Gamma}(\mathbf{r}')\rangle\ . \tag{19}$$

After a little algebra this can be expressed in terms of the previously discussed momentum-density correlation function

$$m^2W(|\mathbf{r}-\mathbf{r}'|)=-\nabla^2\mathrm{Tr}\overleftrightarrow{G}(\mathbf{r}-\mathbf{r}')+\nabla\nabla:\overleftrightarrow{G}(\mathbf{r}-\mathbf{r}')\ , \tag{20}$$

which takes the simple form in k space

$$m^2W(k)=k^2\mathrm{Tr}\overleftrightarrow{G}(\mathbf{k})-\mathbf{kk}:\overleftrightarrow{G}(\mathbf{k})\ . \tag{21}$$

Writing $\overleftrightarrow{G}(\mathbf{r})$ in momentum space as

$$\overleftrightarrow{G}(\mathbf{k})=\int e^{i\mathbf{k}\cdot\mathbf{r}}\overleftrightarrow{G}(\mathbf{r})dr^2=\frac{m}{\beta}[\rho_N(k)\overleftrightarrow{I}+\rho_S(k)\hat{\mathbf{k}}\hat{\mathbf{k}}]\ , \tag{22}$$

the expression for $W(k)$ simplifies to

$$\int W(r)e^{i\mathbf{k}\cdot\mathbf{r}}dr^2=W(k)=\frac{1}{m\beta}k^2\rho_N(k)\ . \tag{23}$$

Figure 13 herein shows $\rho_N(k)$ for a range of temperatures above and below the transition temperature. From Eqs. (7) and (9)

$$\rho_N(k)\rightarrow\begin{cases}\rho_N, & \text{small } k\\ \rho\beta\langle K\rangle, & \text{large } k\ ,\end{cases} \tag{24}$$

and $\rho_N(k)+\rho_S(k)=\rho$ by the f sum rule.[17]

Figure 14 displays the $W(r)$ obtained from the $\rho_N(k)/\rho$ of Fig. 13 using Eq. (23). Very little temperature dependence is seen. All of the structure for $r<3.7$ Å is associated with the vortex core. Vortex unbinding would appear at large r and is apparently below the resolution of this calculation. The question of how to study equilibrium vortices in these types of simulations merits further consideration.

ACKNOWLEDGMENTS

We thank D. J. Thouless for his comments. This work was performed under the auspices of the U.S. Department of Energy by the Lawrence National Laboratory under Contract No. W-7405-ENG-48.

[1]J. M. Kosterlitz and D. J. Thouless, Prog. Low Temp. Phys. **VIIB**, 371 (1978).
[2]D. R. Nelson, *Phase Transitions and Critical Phenomena* (Academic, London, 1983), Vol. 7, p. 1.
[3]P. Minnhagen, Rev. Mod. Phys. **59**, 1001 (1987).
[4]B. I. Halperin, in *Physics of Low-Dimensional Systems,* Proceedings of the Kyoto Summer Institute, Sept. 1979, edited by Y. Nagaoka and S. Hikami (Publications Office, Prog. Theor. Phys., Kyoto, 1979), p. 53.
[5]I. Rudnick, Phys. Rev. Lett. **44**, 1454 (1978); D. J. Bishop and J. Reppy, Phys. Rev. Lett. **40**, 1727 (1978); D. McQueeney, G. Agnolet, and J. D. Reppy, Phys. Rev. Lett. **52**, 1325 (1984).
[6]E. L. Pollock and D. M. Ceperley, Phys. Rev. B **36**, 8343 (1987).
[7]R. A. Aziz, V. P. S. Nain, J. S. Carley, W. L. Taylor, and G. T. McConville, J. Chem. Phys. **70**, 4330 (1979).
[8]P. A. Whitlock, G. V. Chester, and M. H. Kalos, Phys. Rev. B **38**, 2418 (1988).
[9]R. P. Feynman, *Statistical Mechanics* (Benjamin, Reading, MA, 1972).
[10]D. M. Ceperley and E. L. Pollock, Phys. Rev. Lett. **56**, 351 (1986).
[11]D. M. Ceperley and E. L. Pollock (unpublished).
[12]V. Kotsubo and G. A. Williams, Phys. Rev. B **33**, 6106 (1986).
[13]This method using the same vortex core diameter and energy also agrees with ρ_S/ρ values computed for smaller ^{4}He systems. [Doug Peters (private communication)].
[14]I. Rudnick, Phys. Rev. Lett. **40**, 1454 (1978).
[15]D. M. Ceperley and E. L. Pollock, Can. J. Phys. **65**, 1416 (1987).
[16]O. Penrose and L. Onsager, Phys. Rev. **104**, 576 (1956).
[17]Ryogo Kubo and Takeo Nagimaya, *Solid State Physics* (McGraw-Hill, New York, 1969), p. 223.